

PAPER

CrossMark
click for updatesCite this: *RSC Adv.*, 2015, 5, 93684

Ad-layers enhance graphene's performance†

Ting-Wei Chen,^a Ya-Ping Hsieh*^a and Mario Hofmann^b

Graphene, a monoatomic sheet of graphite, could find application as a transparent conducting film (TCF) in solar cells and electronic devices. Currently available graphene, however, does not meet industry requirements in conductivity for these uses. We here demonstrate that ad-layers, discontinuous graphene islands on top of a complete graphene layer, can significantly enhance graphene's TCF-performance. Two routes were employed to produce controllable densities of ad-layers. Electropolishing pretreatment of the catalyst was found to affect the ad-layer nucleation. Alternatively, variation of the growth parameters was employed to influence the density of ad-layer dimensions. By analyzing the coverage-dependent carrier transport, we identified a continuous enhancement even by small ad-layers. This surprising behavior was quantitatively explained by a high conductivity parallel current path through the ad-layers. The resulting ad-layer-covered graphene exhibits a high and tunable performance as a transparent conductor.

Received 15th September 2015

Accepted 27th October 2015

DOI: 10.1039/c5ra18984e

www.rsc.org/advances

Introduction

Graphene is a two-dimensional carbon allotrope that has received significant attention from both fundamental research and applied sciences. One of its major applications is anticipated to be as a transparent conducting film (TCF) in next-generation displays, flexible electronics, and solar cells.^{1,2} The most promising approach to synthesizing high quality graphene on a large scale is chemical vapor deposition (CVD). In the CVD process, a carbon precursor is decomposed over a catalytic substrate and the generated carbon radicals are incorporated into the outgrowing graphene layer.³ A wide range of carbon precursors, catalytic substrates, and growth processes have been investigated in their ability to grow high quality graphene and the most promising approach is the graphene growth from methane on copper substrates.^{4,5} Despite recent progress, the current performance of CVD-graphene TCFs is below industry requirements for many applications.⁶

One approach to improve the limited conductance is by increasing graphene's thickness. Through addition of parallel conduction channels, enhanced carrier conduction can be achieved.⁷ Despite the potential of this method, limited understanding hinders its application. Previous reports on carrier transport through multi-layer graphene restricted

themselves to explaining the conduction by non-interacting channels⁸ and consequently only investigated the conduction through complete bi- and multi-layers. Common CVD methods, however, result in incomplete ad-layers that only partially cover a continuous graphene film, due to details of the growth process.⁹ Since these graphene islands do not form a complete layer, they were assumed to be ineffective for carrier transport and significant effort has been invested into suppressing ad-layer formation.¹⁰

We here demonstrate that ad-layers are enhancing the carrier transport in graphene even at low coverage. Two routes for the controllable formation of graphene ad-layers were developed. First, we demonstrate that modifying the pretreatment of the copper catalyst enables fine control over the graphene continuity and multilayer coverage. Surface bound particles were found to be the origin of graphene grains and their density correlates with high concentration of graphene grains. Control of the particle density facilitates the synthesis of graphene with different morphologies. Second, controlled-pressure (CP)-CVD¹¹ was investigated as an alternative route to producing graphene with controllable ad-layer coverage. The partial pressure of hydrogen was found to determine the ad-layer morphology through its competing effects on carbon radical transport and growth kinetics.

Both methods enable the tuning of graphene ad-layer concentration and we observe that the formation of ad-layers, irrespective of their continuity, is increasing the performance of graphene TCFs. This observation was explained by reexamination of the carrier transport in graphene and high efficiency parallel conduction through the ad-layers was found. Our results open up a new route for the improving the synthesis of graphene TCFs.

^aGraduate Institute of Opto-Mechatronics, National Chung Cheng University, Chiayi, 62102, Taiwan. E-mail: yphsieh@ccu.edu.tw

^bDepartment of Material Science and Engineering, National Cheng Kung University, Tainan, 70101, Taiwan

† Electronic supplementary information (ESI) available: Microscope images and complete Raman spectra, FOM comparison to literature. See DOI: 10.1039/c5ra18984e

Experimental

Copper foil (99.8%, Alfa-Aesar, no. 13382) was electropolished in an electrolyte containing a mixture of 3 : 1 by volume of H_3PO_4 (85%) and PEG ($M_w = 400$, Sigma-Aldrich Co.). A voltage of 3 V was applied between two copper foil electrodes using a Motech LPS 5050N power supply. After polishing, the copper foil serving as the anode was cleaned by rinsing with DI water and isopropyl alcohol and then dried in a stream of N_2 .

Graphene was grown on thus prepared Cu foils by CVD under two different conditions following previous reports.¹² Low pressure (LP)-CVD was carried out by annealing the copper substrates at 1000 °C for 70 minutes under 10 sccm H_2 flow. Graphene growth commenced when a flow of 40 sccm CH_4 was introduced resulting in a total pressure of 7 Torr. After the growth duration of 40 min graphene samples were cooled down to room temperature under a hydrogen flow of 10 sccm. To ensure consistency of the results and minimize the influence of growth variations, all samples were grown in the same batch.

Controlled chamber pressure (CP)-CVD was initiated by annealing the copper substrate at 1050 °C under a hydrogen flow of 500 sccm and a pressure of 1500 Torr for 7 hours.¹³ Growth proceeded at variable CH_4 and H_2 flow rates at a pressure of 100 Torr. After 30 minute growth durations samples were cooled under a flow of 20 sccm hydrogen at 100 Torr.

For characterization of electrical properties, 1 cm^2 graphene samples grown on copper were transferred onto quartz using a polymethyl-metacrylate (PMMA) layer (Microchem A9) as mechanical support following previous reports.¹⁴ FeCl_3 etchant was used to remove the copper foil during the transfer process. Sheet resistance was then measured in van-der-Pauw-geometry using a 4-point probe station.

Transmittance spectra were measured with a KMAC Spectra Academy SV2100 and the figure of merit (FOM) was calculated from transmittance and sheet resistance measurements following De *et al.*¹⁵

Results and discussion

The catalyst morphology is thought to be a significant parameter that determines the graphene morphology and previous reports found a correlation of catalyst flatness and grain size.^{16–18} We here employ electropolishing to modify the catalyst morphology and thus control the ad-layer coverage. In the electropolishing process, field enhancement at protrusions causes faster electrochemical dissolution which results in leveling. Based on this process, large undulations which are an artifact of the copper fabrication process, are successively etched into microscopic particles and finally removed.¹⁹

This evolution can be seen when comparing the series of optical images taken at different times during the electropolishing process. Fig. 1(a) shows copper foil after various polishing duration. Rolling lines are visible for electropolishing times of 20 minutes. After 30 minutes polishing the rolling lines have disappeared and individual particles remain. Finally, after 40 minutes most particles have been removed. Consequently, the particle density evolution over time is determined by the

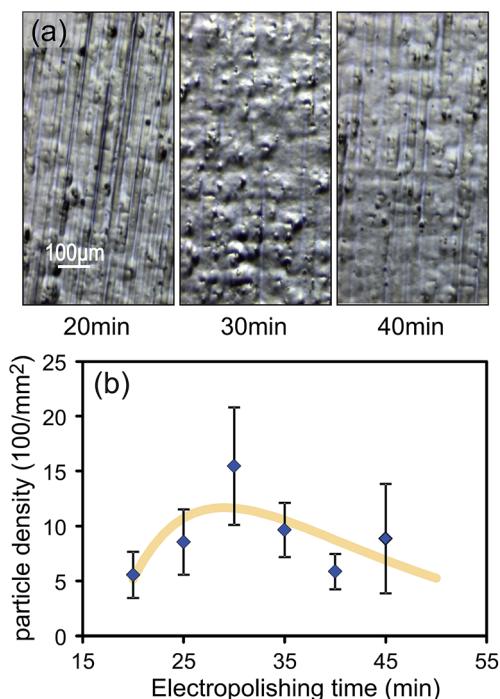


Fig. 1 Effect of electropolishing on catalyst morphology: (a) optical micrographs of Cu foil after various electropolishing durations (b) evolution of particle density with electropolishing time with fit.

conversion of large scale undulations into microparticles and their removal and can be modeled by a rate equation.

$$\frac{dn}{dt} \sim A - n$$

Where n is the number of particles and A is the availability of undulations. The density of undulations itself is decreasing with time through formation of nanoparticles.

$$\frac{dA}{dt} \sim -A$$

The solution of these coupled differential equations describes the density of particles as a function of time, conversion rates (k_1 and k_2) and initial undulation and particle concentrations α , β .

$$n(t) = \alpha \exp(-k_1 t) + \beta^* \exp(-k_2 t)$$

Dark field microscopy (Fig. S1†) was employed to quantify this behavior. Fig. 1(b) shows the extracted particle density as a function of electropolishing time. The good fit of the data to our simple model indicates its suitability.

Copper foil with varying particle densities was subjected to CVD in order to grow graphene. It is found that the particle density is affecting the amount of ad-layers produced after growth. The inset of Fig. 2(a) shows an OM image of graphene grown on 30 minute electropolished Cu which exhibited the highest density of particles (Fig. 1(b)). Many darker areas can be

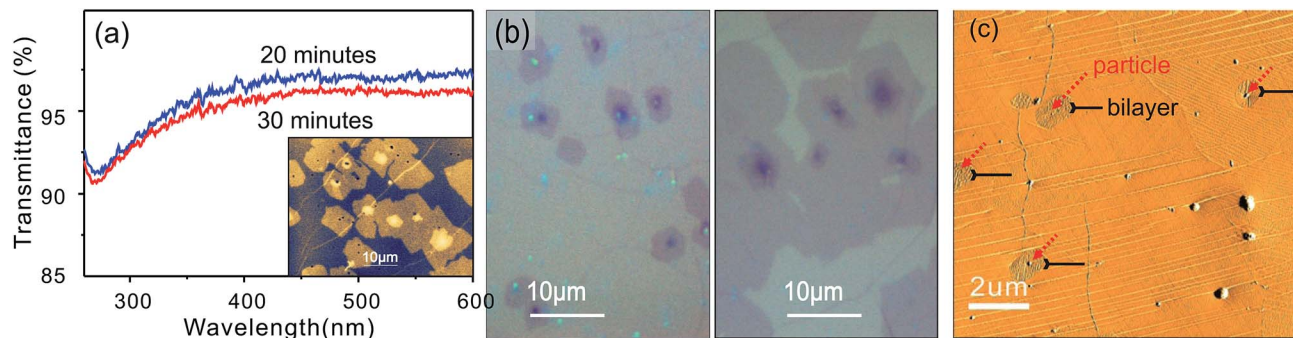


Fig. 2 Evidence for ad-layer formation at high particle densities: (a) comparison of transmittance spectra at different particle densities, (inset) false-color optical micrograph showing ad-layer regions (b) optical micrographs of graphene samples with 10% (left) and 69% (right) ad-layer coverage (c) AFM phase image with indications of ad-layer and nucleation seeds.

seen that represent ad-layer graphene areas which can be also identified from the I_{2D}/I_G ratio of the Raman spectra (see ESI Fig. S2†). Transmittance measurements confirm that the graphene transmittance is lower than the value expected for single layer graphene (Fig. 2(a)).

Optical micrographs indicate that the ad-layers are increasing in both size and density for higher particle concentrations (Fig. 2(b)). To identify the origin of the ad-layers, we conducted atomic force microscopy of graphene on Cu-foil (Fig. 2(c)). Due to different interactions of the substrate with the growing graphene at high temperatures, the Cu texture is highlighting regions of single- and ad-layer graphene.²⁰

At the center of each ad-layer region a particle can be observed indicating that graphene growth originates from these particles in agreement with previous observations.^{21,22}

Based on previously established growth models^{22,23} we hypothesize that carbon radicals diffuse between the copper substrate and the out-growing main layer where they selectively adsorb onto protrusions due to their curvature-induced lowering of the surface free energy. Consequently, supersaturation is preferentially achieved at the particles and they act as nucleation seeds for outgrowing ad-layers. This model is supported by our observation that, while ad-layers were found to be predominantly bilayers, small three- to five-layer islands all nucleated at the same position (Fig. 2(b)).

To confirm this hypothesis, we characterized the ad-layer coverage for samples grown after different electropolishing times. Image processing techniques were employed to identify single ad-layer regions and quantify their surface coverage. The total graphene coverage was then calculated as the sum of main-layer and ad-layer coverage. Fig. 3(a) shows that the ad-layer coverage follows a similar trend with electropolishing time as the particle density. Consequently, the density of ad-layers can be controlled by changing the electropolishing duration.

CP-CVD was employed as a second route to produce controllable densities of ad-layers. We find that the ratio of methane and hydrogen concentration controls the amount ad-layer coverage during growth as shown in Fig. 3(b). This behavior is in agreement with previous reports that found a dual role of hydrogen in facilitating graphene growth at low concentration and etching graphene at high concentrations.²⁴ A simple modeling of the competing effects of hydrogen partial pressure on adsorption and chemical reaction was carried out by fitting a pressure-dependent Freundlich adsorption isotherm and pressure-driven equilibrium concentrations to our data (Fig. 3(b)).

Variable-time electropolishing in combination with LP-CVD and control of the hydrogen partial pressure in CP-CVD provides us with two routes for controlling the ad-layer coverage. When analyzing the impact of ad-layer coverage on

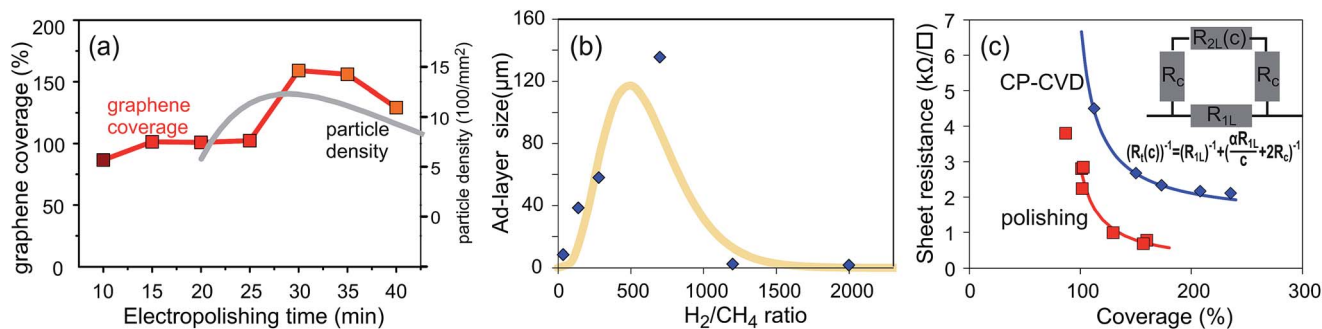


Fig. 3 Tunability of ad-layer coverage: (a) graphene coverage vs. electropolishing time and particle density from Fig. 1(b), (b) ad-layer dimension vs. hydrogen partial pressure in CP-CVD growth. (c) Sheet resistance for graphene films with different ad-layer coverage produced by both methods, (inset) equivalent circuit used for fitting.

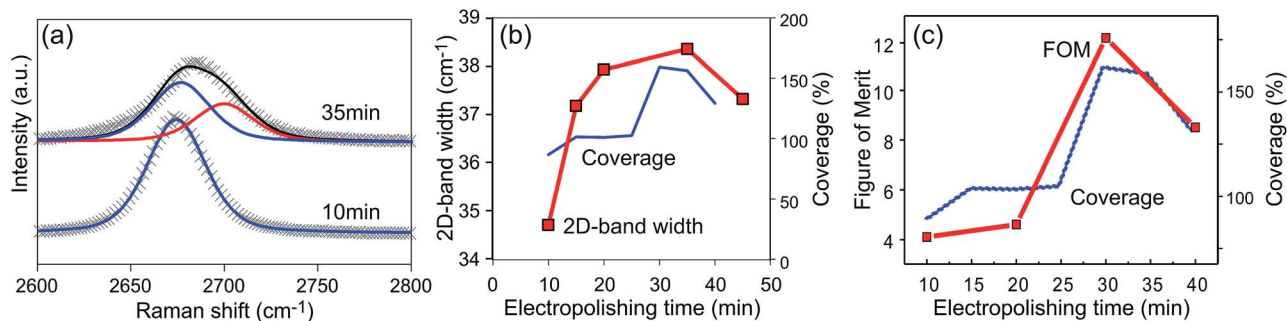


Fig. 4 (a) Deconvolution of Raman 2D-band of graphene grown after different electropolishing times, (b) 2D-band width and coverage vs. electropolishing time, (c) figure of merit and sheet resistance as function of electropolishing time.

top of continuous graphene, we observe a continuous decrease of sheet resistance as the ad-layer concentration increases (Fig. 3(c)). This finding is surprising since, in analogy with graphite, a large out-of-plane resistance between adjacent graphene layers is expected.²⁵ Under such conditions, the addition of discontinuous ad-layer regions would not change the sheet resistance since transport between neighboring layers would be suppressed.

The observed behavior indicates that the ad-layer provides a parallel conduction pathway that lowers the total resistance. The impact of increasing ad-layer coverage on sheet resistance was modeled with a simple lumped circuit model (inset Fig. 3(c)). The continuous single graphene layer was modeled as a constant resistance of value R_{1L} . The change of resistance within the extending ad-layer was approximated by

$$R_{2L} = \frac{\alpha R_{1L}}{c}, \quad (1)$$

where c is the ad-layer coverage and α is introduced to account for differences in conductivity between first and second layer.

Finally, the contact resistance R_c introduces an additional resistance in series with the second layer.

Based on this circuit, the total resistance (R_t) is a function of coverage c :

$$(R_t(c))^{-1} = (R_{1L})^{-1} + \left(\frac{\alpha R_{1L}}{c} + 2R_c \right)^{-1} \quad (2)$$

The suitability of the simple model is indicated by the good fit to the experimental data for both ad-layer production methods (Fig. 3(c)). A value of $36 \Omega \square^{-1}$ was extracted for the contact resistance between neighboring layers produced by the electropolishing method and $900 \Omega \square^{-1}$ for the CP-CVD method. These values are significantly smaller than the extracted in-plane resistances of graphene for both cases. ($R_{1L} = 2841 \Omega \square^{-1}$ and $R_{1L} = 9234 \Omega \square^{-1}$ for electropolishing and CP-CVD, respectively) indicating the non-negligible contribution of the out-of-plane conduction pathway.

The resistance of the second flake was found to be lower than the first one as indicated by the extracted value of α around 0.17% for both methods. A complete ad-layer would consequently exhibit a $6\times$ lower resistance than the first layer.

To understand this behavior, we carried out Raman characterization of the graphene with different ad-layer coverage. We find that the defect induced D-band feature does not change with an increased ad-layer coverage, suggesting that the number of structural defects is not affected by the increased nucleation density of ad-layers (Fig. S2†). Interestingly, however, the 2D-band feature exhibits a significant broadening (Fig. 4(a)). This change was found to originate from an overlap of the Raman signal of the main layer and the ad-layer. A blue shift between the original peak and the second occurring peak suggests that the ad-layer is more heavily p-type doped than the main layer.²⁶ The higher doping within the ad-layer explains the observed enhanced conductivity compared to the main layer in agreement with the carrier transport results. We furthermore observe a clear correlation between the 2D-band peak width and the ad-layer coverage corroborating our explanation (Fig. 4(b)).

We therefore conclude that graphene ad-layers exhibit a higher conductivity due to a larger doping that may originate from interaction with the substrate²⁷ or from adsorbates.²⁸ The higher achievable doping of this bilayer arrangement compared to a single-layer could be due to an increased adsorbate density at the ad-layer edges.²⁹

The significance of our findings is illustrated when comparing the performance of graphene TCFs obtained after different electropolishing time: samples that were polished for 30 minutes and have high ad-layer densities exhibit FOMs which are three times higher than single layer graphene (Fig. 4(c)).

Future studies have to elucidate if the observed values could be even more enhanced by combining the optimization of graphene morphology with optimizing the transfer process.

Conclusions

In conclusion, the impact of ad-layers on the performance of CVD grown graphene was investigated. Electropolishing was employed to control the density of nucleation seeds for graphene ad-layers. Changing the hydrogen concentration at relatively high pressures was used as a second route to control the ad-layer density. Surprisingly the grown ad-layers are enhancing the carrier transport by providing a low resistance parallel conduction pathway. The performance of graphene TCFs was

found to scale with the ad-layer concentration and a smooth transition in the resistance between the values of complete single-layer and bi-layers was observed. These results highlight the potential of tailoring the morphology of graphene for future applications.

Acknowledgements

YP Hsieh and M. Hofmann acknowledges financial support from Applied Materials, Inc., the Ministry of Science and Technology (NSC-102-2112-M-194-003-MY3 and NSC-104-2112-M-006-013-MY3), and Industrial Technology Research Institute of Taiwan.

References

- 1 K. S. Novoselov, V. I. Fal'ko, L. Colombo, P. R. Gellert, M. G. Schwab and K. Kim, *Nature*, 2012, **490**, 192–200.
- 2 M. J. Cha, S. M. Kim, S. J. Kang, J. H. Seo and B. Walker, *RSC Adv.*, 2015, **5**, 65646–65650.
- 3 X. Li, W. Cai, J. An, S. Kim, J. Nah, D. Yang, R. Piner, A. Velamakanni, I. Jung, E. Tutuc, S. K. Banerjee, L. Colombo and R. S. Ruoff, *Science*, 2009, **324**, 1312–1314.
- 4 M. Losurdo, M. M. Giangregorio, P. Capezuto and G. Bruno, *Phys. Chem. Chem. Phys.*, 2011, **13**, 20836–20843.
- 5 Z. Sun, Z. Yan, J. Yao, E. Beitler, Y. Zhu and J. M. Tour, *Nature*, 2010, **468**, 549–552.
- 6 S. De and J. N. Coleman, *ACS Nano*, 2010, **4**, 2713–2720.
- 7 S. Bae, H. Kim, Y. Lee, X. Xu, J. S. Park, Y. Zheng, J. Balakrishnan, T. Lei, H. R. Kim, Y. I. Song, Y. J. Kim, K. S. Kim, B. Ozyilmaz, J. H. Ahn, B. H. Hong and S. Iijima, *Nat. Nanotechnol.*, 2010, **5**, 574–578.
- 8 J. Nilsson, A. C. Neto, F. Guinea and N. Peres, *Phys. Rev. B: Condens. Matter Mater. Phys.*, 2008, **78**, 045405.
- 9 J. Ning, D. Wang, D. Han, Y. Shi, W. Cai, J. Zhang and Y. Hao, *J. Cryst. Growth*, 2015, **424**, 55–61.
- 10 B. Dai, L. Fu, Z. Zou, M. Wang, H. Xu, S. Wang and Z. Liu, *Nat. Commun.*, 2011, **2**, 522.
- 11 W. Wu, Q. Yu, P. Peng, Z. Liu, J. Bao and S. S. Pei, *Nanotechnology*, 2012, **23**, 035603.
- 12 X. Li, W. Cai, J. An, S. Kim, J. Nah, D. Yang, R. Piner, A. Velamakanni, I. Jung and E. Tutuc, *Science*, 2009, **324**, 1312–1314.
- 13 Z. Yan, J. Lin, Z. Peng, Z. Sun, Y. Zhu, L. Li, C. Xiang, E. L. Samuel, C. Kittrell and J. M. Tour, *ACS Nano*, 2012, **6**, 9110–9117.
- 14 K. K. Kim, A. Reina, Y. Shi, H. Park, L. J. Li, Y. H. Lee and J. Kong, *Nanotechnology*, 2010, **21**, 285205.
- 15 S. De and J. N. Coleman, *ACS Nano*, 2010, **4**, 2713–2720.
- 16 S. Dhingra, J.-F. Hsu, I. Vlassioug and B. D'Urso, *Carbon*, 2014, **69**, 188–193.
- 17 C. Jia, J. Jiang, L. Gan and X. Guo, *Sci. Rep.*, 2012, **2**, 707.
- 18 Z. Luo, Y. Lu, D. W. Singer, M. E. Berck, L. A. Somers, B. R. Goldsmith and A. T. C. Johnson, *Chem. Mater.*, 2011, **23**, 1441–1447.
- 19 J. Huo, *Electrochemical planarization of copper for microelectronic applications*, 2004, Scholar Archive, Paper 209.
- 20 K. Celebi, M. T. Cole, J. W. Choi, F. Wyczisk, P. Legagneux, N. Rupesinghe, J. Robertson, K. B. Teo and H. G. Park, *Nano Lett.*, 2013, **13**, 967–974.
- 21 L. Gan and Z. Luo, *ACS Nano*, 2013, **7**, 9480–9488.
- 22 Q. Li, H. Chou, J. H. Zhong, J. Y. Liu, A. Dolocan, J. Zhang, Y. Zhou, R. S. Ruoff, S. Chen and W. Cai, *Nano Lett.*, 2013, **13**, 486–490.
- 23 W. Fang, A. L. Hsu, Y. Song, A. G. Birdwell, M. Amani, M. Dubey, M. S. Dresselhaus, T. Palacios and J. Kong, *ACS Nano*, 2014, **8**, 6491–6499.
- 24 I. Vlassioug, M. Regmi, P. Fulvio, S. Dai, P. Datskos, G. Eres and S. Smirnov, *ACS Nano*, 2011, **5**, 6069–6076.
- 25 W. Primak, *Phys. Rev.*, 1956, **103**, 544–546.
- 26 A. Das, S. Pisana, B. Chakraborty, S. Piscanec, S. K. Saha, U. V. Waghmare, K. S. Novoselov, H. R. Krishnamurthy, A. K. Geim, A. C. Ferrari and A. K. Sood, *Nat. Nanotechnol.*, 2008, **3**, 210–215.
- 27 Y. Zhang, V. W. Brar, C. Girit, A. Zettl and M. F. Crommie, *Nat. Phys.*, 2009, **5**, 722–726.
- 28 F. Gunes, H. J. Shin, C. Biswas, G. H. Han, E. S. Kim, S. J. Chae, J. Y. Choi and Y. H. Lee, *ACS Nano*, 2010, **4**, 4595–4600.
- 29 H. Terrones, R. Lv, M. Terrones and M. S. Dresselhaus, *Rep. Prog. Phys.*, 2012, **75**, 062501.